# Image-Driven Spatial Interpolation with Deep Learning for Radio Map Construction

Katsuya Suto, *Member, IEEE,* Shinsuke Bannai, *Student Member, IEEE,* Koya Sato, *Member, IEEE,* Kei Inage, *Member, IEEE,* Koichi Adachi, *Senior Member, IEEE,* Takeo Fujii, *Member, IEEE*

***Abstract*—Radio maps are a promising technology that can boost the capability of wireless networks by enhancing spectrum efficiency. Since spatial interpolation is a critical challenge to construct a precise radio map, the latest works have proposed deep learning (DL)-based interpolation methods. However, a DL model that achieves enough estimation accuracy for practical uses has not yet been established due to the complexity of radio propagation characteristics. Therefore, we propose a novel DL framework that transforms the spatial interpolation problem into a shadowing adjustment problem suitable for DL-based approaches. We evaluate the performance using real measurement data in urban and suburban areas to show that the proposed framework outperforms the state-of-the-art deep learning models.**

## I. Introduction

RADIO maps enable the reuse of the spectrum hole in space and power domains so that transmitters cognitively perform spectrum sharing [1] and interference management [2]. Further, radio maps could be a crucial technology for improving the robustness of positioning and localization systems [3].

Although deploying numerous sensor nodes is an easy way to construct a precise radio map, it may incur extravagant costs. Hence, spatial interpolation with limited sensors is expected to play an indispensable role in practical radio map construction. The latest works have been focused on machine learning (ML) and deep learning (DL), which can be divided into data-driven approaches [4]–[7] or image-driven approaches [8]–[12].

Data-driven approaches aim to develop a precise regression model in which deep feedforward networks are used to express the correlation between the path loss/shadowing and site-specific parameters such as a crossed clutter factor [4] and a building height [5]. In [6], such DL-based regression has been extended by using convolutional neural networks (CNN) to extract site-specific parameters from a satellite image of the measurement area. Kriging and Gaussian process regression have been widely used to estimate the spatial distribution of received signal power [7]. The mechanism behind these approaches is to treat scalar values as input to estimate the path loss and shadowing (also scalar values) at arbitrary points.

The main idea of image-driven approaches is to treat the radio propagation data as an image and develop the spatial interpolation method with image processing techniques. Different from data-driven approaches, image-driven approaches utilize the matrices as input and output data. These approaches have attracted much attention since they skillfully estimate the spatial distribution of received signal power. Nearest neighbor (NN) methods such as $k$-NN and weighted $k$-NN are widely used for spatial interpolation [8], [9]. Y. Deng *et al.* [10] have proposed a spatial interpolation method using super-resolution combined with Kriging interpolation, dictionary learning, and random forest. The work [11] has demonstrated that super-resolution CNN models are effective for the spatial interpolation problem in radio map construction. In work [12], an image-driven spatial interpolation based on the state-of-the-art generative adversarial networks (GAN) has been proposed.

However, the existing DL models cannot express both the path loss and shadowing fluctuations since they have different characteristics. To address the issue, we propose a novel DL model for the image-driven spatial interpolation problem. We transform the spatial interpolation problem into a shadowing adjustment problem and introduce a neural network (NN) structure suitable for the shadowing adjustment problem. Furthermore, we propose a gradual train method (GTM) that stably obtains the optimal parameter of NN. We demonstrate that the proposed framework outperforms the latest image-driven approaches [11], [12] through performance evaluation using measurement datasets in urban and suburban areas.

## II. System Model and Objective

A radio map is defined as a map storing the spatial distribution of received signal strength from a transmitter emitting radio waves over a specific carrier frequency. A database collects the received signal strength and location information from the user terminals to construct a radio map. All the instantaneous data are averaged for each grid, i.e., an exclusive division of several hundred square meters, to alleviate the multipath fading effect. With the procedure, we obtain a location-dependent value for each grid.

Considering that some grids do not store the received signal strength, we have an imperfect radio map, denoted by

This research is supported by the Ministry of Internal Affairs and Communications in Japan (JPJ000254).

K. Suto is with the Graduate School of Informatics and Engineering, The University of Electro-Communications, Chofu, Tokyo, JAPAN. e-mail: k.suto@uec.ac.jp.

S. Bannai is with the Department of Computer and Network Engineering, The University of Electro-Communications, Chofu, Tokyo, JAPAN. e-mail: s.bannai@uec.ac.jp.

K. Sato is with the Department of Electrical Engineering, Tokyo University of Science, Katsuhika-ku, Tokyo, JAPAN. e-mail:k_sato@ieee.org

K. Inage is with the Tokyo Metropolitan College of Industrial Technology, Shinagawa City, Tokyo, JAPAN. e-mail: inage@metro-cit.ac.jp

K. Adachi and T. Fujii are with the Advanced Wireless and Communication Research Center (AWCC), The University of Electro–Communications, Chofu, Tokyo, JAPAN. e-mail: {adachi, fujii}@awcc.uec.ac.jp

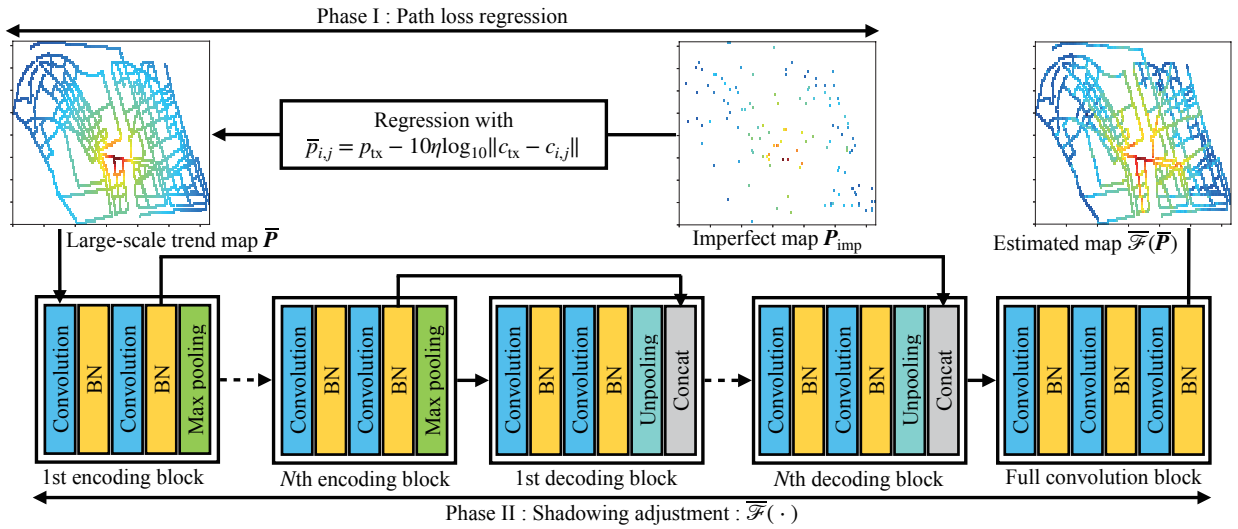


Fig. 1. Illustration of the proposed interpolation model.

$\boldsymbol{P}_{\text{imp}} \in \mathbb{R}^{n_{\text{c}} \times n_{\text{r}}}$, where $n_{\text{c}}$ and $n_{\text{r}}$ are the numbers of grids in columns and rows of $\boldsymbol{P}_{\text{imp}}$. Furthermore, $p_{i,j}$ represents the received signal strength with normalization for the grid-$(i,j)$. For the following three grids types, we set $p_{i,j}$ to different values: The range of measured grids is $[0,1]$, i.e., $p_{i,j} \in [0,1]$. We set $p_{i,j}$ to 0 for unmeasured grids whose radio propagation information is not measured. Since the propagation characteristics of the obstruction grids in which buildings exist are different from the measured grids, we set their value to $-1$, i.e., $p_{i,j} = -1$, to ignore the spatial interpolation at those grids.

The objective of this letter is to interpolate the received signal strength of the unmeasured grids. More specifically, we aim to obtain the mapping model $\mathcal{F}$ from the imperfect map $\boldsymbol{P}_{\text{imp}}$ to the ground truth $\boldsymbol{P}$.

$$\mathcal{F} : \boldsymbol{P}_{\text{imp}} \rightarrow \boldsymbol{P}. \tag{1}$$

In reality, measured grids account for less than 10 % of all the grids [12]. In such a sparse measurement environment, it is very challenging to derive an accurate mapping model for the following reasons: (i) The correlation distance and variance of shadowing fluctuation depend on the locations. (ii) Spatial interpolation with distant grids results in large estimation errors. (iii) The location patterns of grids affect mapping accuracy. We, therefore, investigate how to derive the mapping model using deep learning techniques.

## III. Proposed Framework

As illustrated in Fig. 1, we propose a novel framework that transforms the spatial interpolation problem into a shadowing adjustment problem. Furthermore, we introduce a NN structure suitable for the shadowing adjustment problem and a novel training method that decides the optimal weight set for windows step-by-step.

### A. Problem transformation

Due to the difficulty of the non-linear mapping from sparse data, we transform the spatial interpolation problem defined in Eq. (1) into a shadowing adjustment problem. To this end, we estimate the large-scale trend of received signal power at grid-$(i,j)$, $\overline{p}_{i,j}$, which contains the transmission power, the antenna gain, and the path loss, by using the following regression equation[1]:

$$\overline{p}_{i,j} = p_{\text{tx}} - 10\eta\log_{10}\|c_{\text{tx}} - c_{i,j}\|, \tag{2}$$

where $p_{\text{tx}}$ is the transmission power, including the antenna gain, $\eta$ is the path loss index, $\|\cdot\|$ denotes the Euclidean distance, and $c_{\text{tx}}$ and $c_{i,j}$ are the locations of the transmitter and grid-$(i,j)$, respectively. Additionally, $p_{\text{tx}}$ and $\eta$ can be estimated by fitting (2) using ordinary least squares (OLS) with the measurement data in the imperfect map $\boldsymbol{P}_{\text{imp}}$. With the model, we construct a large-scale trend map $\overline{\boldsymbol{P}}$, where $\overline{p}_{i,j}$ is an element of $\overline{\boldsymbol{P}}$. Let $\sigma_{i,j}$ be the magnitude of shadowing at grid-$(i,j)$. Since the received signal power at grid-$(i,j)$ can be expressed as

$$p_{i,j} = \overline{p}_{i,j} + \sigma_{i,j}, \tag{3}$$

we have to estimate the magnitude of shadowing $\sigma_{i,j}$. Thus, the transformed problem aims to obtain the mapping model $\overline{\mathcal{F}}$ from the large-scale trend map $\overline{\boldsymbol{P}}$ to the ground truth $P$.

$$\overline{\mathcal{F}} : \overline{\boldsymbol{P}} \rightarrow \boldsymbol{P}. \tag{4}$$

### B. Neural network structure for shadowing adjustment

Although the problem transformation makes deep learning easier, the mapping model is still complex due to shadowing effects' intricacy. Hence, we introduce a multiple encoding/decoding (ED) blocks structure [14] to express the complex feature of shadowing. Since the NN is used for image segmentation, it works well to classify the measured grid and

[1]We employ a logarithmic function for the regression because the shadowing has a spatial correlation in logarithmic domain [13]. By training the difference between the large-scale trend and the received signal power, the proposed DL model can understand the shadowing fluctuation between neighbors and obtain the mapping function following a clear spatial correlation.

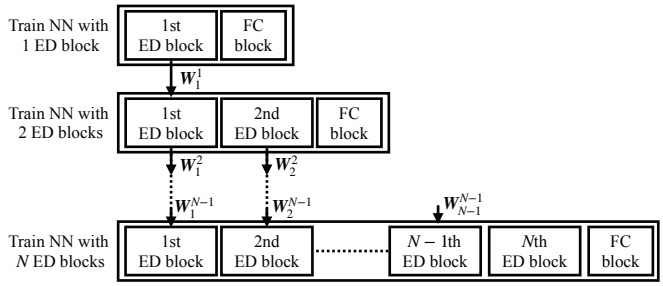


Fig. 2. The proposed training method that gradually trains the ED blocks to obtain a stable NN.

obstruction grid. That is why we employ the NN structure for the shadowing adjustment problem.

As shown in Fig. 1, the structure consists of $N$ encoding blocks, $N$ decoding blocks, and a full convolution (FC) block. Encoding blocks perform two sets of convolution with a $3 \times 3$ window, stride 1, and padding 1, and batch normalization (BN). Further, element-wise rectified-linear non-linearity (ReLU), i.e., $\max(0, x)$, is applied as the activation function. With the procedure, we have a map $\boldsymbol{A}^k \in \mathbb{R}^{n_c/(2^k) \times n_r/(2^k)}$ at the $k$-th encoding block, which is stored in memory and concatenated in the decoding process. Then, max pooling with a $2 \times 2$ window and stride 2 is applied to halve the size of $\boldsymbol{A}^k$. With $N$ encoding blocks, we obtain the feature map of $\overline{\boldsymbol{P}}$, $\overline{\boldsymbol{P}}_{\text{enc}} \in \mathbb{R}^{n'_c \times n'_r}$, where $n'_c = n_c/(2^N)$ and $n'_r = n_r/(2^N)$.

Decoding blocks have two convolution and BN functions similar to the encoding blocks. Different to the encoding blocks, the decoding blocks perform unpooling with a $2 \times 2$ window and stride 2 to double the map size, where the value of each grid in $m$-th decoding blocks is copied to four neighbor grids in the unpooling process. Thus, we have a feature map $\boldsymbol{B}^m \in \mathbb{R}^{2^m n'_c \times 2^m n'_r}$ at the $m$-th decoding block. Additionally, we concatenate $\boldsymbol{B}^m$ and $\boldsymbol{A}^{N-m+1}$ to separate measured grids and obstruction grids. After the $N$-th decoding block, we obtain the restored map of $\overline{\boldsymbol{P}}_{\text{enc}}$, $\overline{\boldsymbol{P}}_{\text{dec}} \in \mathbb{R}^{n_c \times n_r}$.

Although the structure with ED blocks expresses the complex feature of shadowing, it sometimes yields noise. Thus, the FC block performs denoising and smoothing with three convolutions and BN operations. With these three types of blocks, we finally obtain the estimated map $\overline{\mathcal{F}}(\overline{\boldsymbol{P}})$.

### C. Gradual training method

The multiple ED blocks enhance the ability to express the complex feature of shadowing; however, the stability of learning decreases as $N$ increases. To cope with the issue, we propose a gradual training method (GTM) that separately trains each ED block in $N$ training phases, as shown in Fig. 2. More specifically, we first train the NN composed of one ED block and one FC block and store the trained window weights of the first ED block, $\boldsymbol{W}_1^1$. The parameter $\boldsymbol{W}_1^1$ is used as initial window weights of the first ED block in the NN composed of two ED blocks and one FC block. In this way, the trained window weights of the first ED block to $(N-1)$-th ED block, $\{\boldsymbol{W}_1^{N-1}, \cdots, \boldsymbol{W}_{N-1}^{N-1}\}$, are used as initial weights in the $N$ ED blocks training. In other words, the parameters of only the $N$-th ED block and FC block are trained in the $N$ ED blocks training. Compared with the traditional training method that trains all the ED blocks and the FC block at the same time, the proposed training method can achieve higher stability.

## IV. Performance Evaluation

In this section, we verify the performance of the proposed framework using real measurement data in urban and suburban areas, comparing it with existing image-driven DL methods, i.e., GAN-based model [12] and spatial interpolation with convolutional neural networks (SICNN) [11]. All the DL models are implemented by Python 3.7.4 and Chainer 7.4.0 in Ubuntu 18.04.

### A. Dataset and parameters

We use two radio propagation datasets, which are measured in typical urban and suburban areas in Tokyo. Fig. 3(a) shows the radio map constructed by the urban dataset, where the grid size is 10 m × 10 m. A transmitter of 17.5 m height is located at latitude 35.697893 and longitude 139.751289. Continuous waves are emitted over 2115 MHz band via an omnidirectional antenna with transmission power of 35 dBm and gain of 2 dBi. A reception antenna of 2.15 dBi gain is fixed to the cart at 1.5 m height to measure the instantaneous received signal power at 122163 different points. Fig. 4(a) demonstrates the radio map constructed by the suburban dataset. A transmitter is deployed at latitude 35.65751675 and longitude 139.54388671, and its height is 53.7 m. The transmission power and antenna gain are 37 dBm and 2.15 dBi, respectively. A receiver with an antenna of 2.15 dBi gain and 1.7 m height moves around the transmitter to collect 271953 samples.

The hyperparameters of the proposed DL model are summarized below. Weights of NN are decided based on the He initialization [15]. We use Adam as an optimizer. Since the proposed GTM can achieve stable training without any learning rate update methods such as AdaGrad [16], we set the learning rate to 0.0005. We use the imperfect map consisting of $20 \times 20$ grids, and the maximum number of ED blocks is 4 in this case. Since the deeper NN can express the shadowing, we utilize 4 ED blocks in the performance evaluation. We train each ED block for 125 epochs; thus, the total number of epochs is 500. We use the mean squared error (MSE) as the loss function, where the loss is summed up over all grids in each mini-batch.

### B. Estimation results in urban environment

Fig. 3 depicts the examples of radio maps in the urban environment. We divide the true radio map into 24 divided maps consisting of $20 \times 20$ grids as shown in Fig. 3(a). We use the divided maps depicted by black boxes for supervised data and the other divided maps depicted by magenta boxes for performance evaluation. We construct 10 imperfect maps for each divided area by choosing 10 measured grids from each divided area in a random manner. Thus, we have 170 and 70 imperfect maps for training and estimation, respectively. The

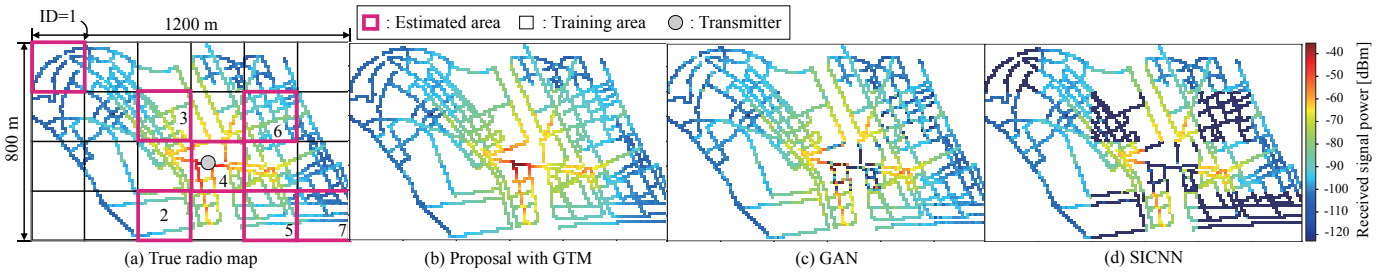


(a) True radio map (b) Proposal with GTM (c) GAN (d) SICNN

Fig. 3. Illustration of radio maps in the urban environment. The true radio map is used for both training and estimation. The number of measured grids in each divided area is 10.

TABLE I
RMSE [dB] OF EACH DIVIDED AREA IN THE URBAN ENVIRONMENT, WHERE THE NUMBER OF MEASURED GRIDS IS 10.

| Area ID | Proposal w/ GTM | Proposal w/o GTM | GAN [12] | SICNN [11] |
|---|---|---|---|---|
| 1 | 2.639 | 28.387 | 5.830 | 88.148 |
| 2 | 3.303 | 3.484 | 6.176 | 86.331 |
| 3 | 6.438 | 33.755 | 8.203 | 99.091 |
| 4 | 8.681 | 8.733 | 65.003 | 103.388 |
| 5 | 5.794 | 5.870 | 7.272 | 90.314 |
| 6 | 5.601 | 31.299 | 17.329 | 102.132 |
| 7 | 3.996 | 4.072 | 6.356 | 91.467 |

TABLE II
AREA-AVERAGED RMSE [dB] FOR DIFFERENT MEASURED GRIDS IN THE URBAN ENVIRONMENT.

| Measured grids | Proposal w/ GTM | Proposal w/o GTM | GAN [12] | SICNN [11] |
|---|---|---|---|---|
| 10 | 5.21 | 16.51 | 16.60 | 94.41 |
| 30 | 5.10 | 8.87 | 14.17 | 71.55 |
| 50 | 5.08 | 9.21 | 11.64 | 57.54 |

TABLE III
AREA-AVERAGED RMSE [dB] IN THE URBAN ENVIRONMENT WITH MEASUREMENT NOISE, WHERE THE NUMBER OF MEASURED GRIDS IS 50.

| Noisy grids | Proposal w/ GTM | Proposal w/o GTM | GAN [12] | SICNN [11] |
|---|---|---|---|---|
| 5 (10%) | 5.072 | 9.178 | 11.659 | 97.373 |
| 15 (30%) | 5.089 | 9.283 | 11.660 | 96.309 |
| 25 (50%) | 5.070 | 9.252 | 11.658 | 97.608 |

training dataset is shuffled to create 17 mini-batches consisting of 10 divided imperfect maps.

Table I shows the root mean square error (RMSE) in dB between the estimated data and ground truth of each estimation area. Five trained NNs are used to evaluate the average RMSE. Although the performance of the proposed model degrades in some areas, it can skillfully express the feature of shadowing, especially in areas 1, 2, and 7. This result causes because the path loss fluctuation is gradual in these areas. Meanwhile, the performance of the proposed DL model without GTM is deficient in areas 1 and 6 because the training without GTM is not stable. From this result, we can confirm the effectiveness of the proposed GTM. GAN cannot express the feature of shadowing and path loss in areas 4 and 6 (See Fig. 3(c)). Although GAN utilizes the learning rate update method ($0.95^{\text{epochs}-1}$) for stable training, it causes underfitting. From this result, we can see that the discriminator-based DL model is not effective in expressing the fine fluctuation of shadowing. SICNN cannot estimate both shadowing and path loss in any areas. Three convolution layers are not enough to express the complex feature of radio propagation.

Table II shows the impact of measured grids on the area-averaged RMSE. Proposal with GTM achieves the lowest RMSE regardless of measured grids while the conventional methods decrease the RMSE as the number of measured grids decreases. Since the proposal obtains the feature of the large-scale trend map with encoding processes, the regression error in low measurement density can be mitigated. Hence, the proposal with GTM is robust to the measurement density.

Table III shows the impact of measurement noise on the area-averaged RMSE. We model the measurement noise model using a log-normal distribution because the received signal strength changes in logarithmic domain due to the noise of sensing terminals [17]. Specifically, the measurement noise of measured grids-$(i,j)$ in logarithmic domain, $p_{i,j}^{\text{noise}}$, follows the normal distribution, $p_{i,j}^{\text{noise}} \sim \mathcal{N}(p_{i,j}, 0.1 \times p_{i,j})$. We also consider that $\{5, 15, 25\}$ grids are affected by the measurement noise. From this result, the proposal and GAN are immune to the measurement noise. However, SICNN significantly decreases the performance due to the measurement noise.

### C. Estimation results in suburban environment

Fig. 4 demonstrates the examples of radio maps in the suburban environment. Similarly to the urban environment, we divide the true radio map into 16 divided maps, in which 7 divided maps depicted by magenta boxes are used for estimation. We use the NNs that are trained by the divided maps in the urban environment.

Table IV shows the RMSE of each divided area whose measured grids is 10. The proposal with GTM expresses the shadowing feature with small measurement data in the suburban area. However, the overall RMSE is increased by around 2 dB, compared with the urban environment. The performance degradation causes due to the following reasons: (i) The feature of shadowing is different between the urban and suburban environments. (ii) Since the path loss fluctuation in the suburban environment is more gradual than in the urban environment, the feature of input data is different in the training phase and estimation phase, yielding the performance degradation. Although GAN estimates the received signal

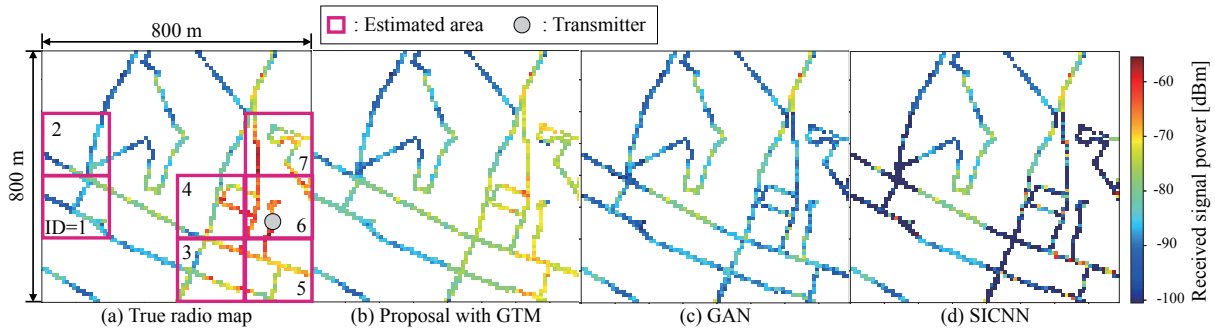


Fig. 4. Illustration of radio maps in the suburban environment. Each DL model is trained by the urban radio map. The number of measured grids in each area is 10.

TABLE IV
RMSE [dB] OF EACH DIVIDED AREA IN THE SUBURBAN ENVIRONMENT, WHERE THE NUMBER OF MEASURED GRIDS IS 10.

| Area ID | Proposal w/ GTM | Proposal w/o GTM | GAN [12] | SICNN [11] |
|---|---|---|---|---|
| 1 | 5.649 | 10.015 | 8.267 | 31.219 |
| 2 | 5.454 | 7.310 | 6.979 | 26.659 |
| 3 | 8.147 | 8.600 | 15.533 | 36.175 |
| 4 | 7.228 | 7.667 | 14.356 | 30.345 |
| 5 | 4.806 | 5.603 | 15.922 | 30.142 |
| 6 | 9.600 | 14.398 | 23.613 | 40.940 |
| 7 | 8.315 | 10.127 | 18.774 | 36.021 |

TABLE V
AREA-AVERAGED RMSE [dB] FOR DIFFERENT MEASURED GRIDS IN THE SUBURBAN ENVIRONMENT.

| Measured grids | Proposal w/ GTM | Proposal w/o GTM | GAN [12] | SICNN [11] |
|---|---|---|---|---|
| 10 | 7.029 | 9.103 | 14.778 | 33.071 |
| 30 | 6.3990 | 8.975 | 14.359 | 26.907 |
| 50 | 6.273 | 9.582 | 14.319 | 22.193 |

strength with acceptable accuracy in areas 1 and 2, it cannot express the path loss in other areas.

Table V shows area-averaged RMSE comparison in the different number of measured grids. The proposal with GTM outperforms the existing DL models. The improvements are 3.309 dB, 8.046 dB, and 15.92 dB, compared with the proposal without GTM, GAN, and SICNN. Further, the proposal decreases the RMSE as the number of measured grids increases. This phenomenon occurs because the proposed model with GTM utilizes the large-scale trend map, whose accuracy can be improved by increasing the number of measured grids. It can be concluded that we can apply the proposed DL model that is trained by the urban dataset to the radio map construction in the suburban area with a few measurement data of the suburban area.

## V. Conclusion

In this letter, we have proposed a novel DL framework for the spatial interpolation problem in radio map constructions. The proposed framework transforms the spatial interpolation problem into a shadowing adjustment problem by using path loss regression and learns the shadowing effect through an encoding/decoding model. Further, we have proposed a novel training method that is suitable for the encoding/decoding model. Using a real measurement dataset, we have verified that the proposal can be superior to the existing DL models.

## References


[1] H. R. Karimi, "Geolocation databases for white space devices in the UHF TV bands : Specification of maximum permitted emission levels," in *Proc. IEEE DySPAN 2011*, Aachen, Germany, May 2011, pp. 443–454.

[2] J. Perez-Romero, *et al.*, "On the use of radio environment maps for interference management in heterogeneous networks," *IEEE Commun. Mag.*, vol. 53, no. 8, pp. 184–191, Aug. 2015.

[3] Q. Jiang, *et al.*, "A probabilistic radio map construction scheme for crowdsourcing-based fingerprinting localization," *IEEE Sensors J.*, vol. 16, no. 10, pp. 3764–3774, Feb. 2016.

[4] M. Ayadi, A. Ben Zineb, and S. Tabbane, "A UHF path loss model using learning machine for heterogeneous networks," *IEEE Trans. Antennas Propag.*, vol. 65, no. 7, pp. 3675–3683, May 2017.

[5] J. Thrane, *et al.*, "Drive test minimization using deep learning with bayesian approximation," in *Proc. IEEE VTC 2018*, Chicago, IL, USA, Aug. 2018, pp. 1–5.

[6] J. Thrane, D. Zibar, and H. L. Christiansen, "Model-aided deep learning method for path loss prediction in mobile communication systems at 2.6 ghz," *IEEE Access*, vol. 8, pp. 7925–7936, Jan. 2020.

[7] K. Sato, K. Inage, and T. Fujii, "On the performance of neural network residual Kriging in radio environment mapping," *IEEE Access*, vol. 7, pp. 94 557–94 568, July 2019.

[8] D. Denkovski, *et al.*, "Reliability of a radio environment map: Case of spatial interpolation techniques," in *Proc. CROWNCOM 2012*, Stockholm, Sweden, June 2012, pp. 248–253.

[9] M. Pesko, *et al.*, "Radio environment maps: The survey of construction methods," *KSII Trans. Internet and Information Systems*, vol. 8, no. 11, pp. 3789–3809, 2014.

[10] Y. Deng, *et al.*, "Radio environment map construction using super-resolution imaging for intelligent transportation systems," *IEEE Access*, vol. 8, pp. 47 272–47 281, Mar. 2020.

[11] R. Hashimoto and K. Suto, "SICNN : Spatial interpolation with convolutional neural networks for radio environment mapping," in *Proc. ICAIIC 2020*, Fukuoka, Japan, Feb. 2020, pp. 167–170.

[12] Z. Li, *et al.*, "Sparsely self-supervised generative adversarial nets for radio frequency estimation," *IEEE J. Sel. Areas Commun.*, vol. 37, no. 11, pp. 2428–2442, Aug. 2019.

[13] M. Gudmundson, "Correlation model for shadow fading in mobile radio systems," *Electron. Lett.*, vol. 27, no. 23, pp. 2145–2146, Nov. 1991.

[14] O. Ronneberger, P. Fischer, and T. Brox, "U-net: Convolutional networks for biomedical image segmentation," in *Proc. MICCAI 2015*, vol. 9351, Munich, Germany, Oct. 2015, pp. 234–241.

[15] K. He, *et al.*, "Delving deep into rectifiers : Surpassing human-level performance on imagenet classification," in *Proc. ICCV 2015*, Santiago, Chile, Dec. 2015, pp. 1026–1034.

[16] L. Luo, *et al.*, "Adaptive gradient methods with dynamic bound of learning rate," in *Proc. ICLR 2019*, New Orleans, Louisiana, May 2019, pp. 1–21.

[17] Z. Fang, *et al.*, "Rssi variability characterization and calibration method in wireless sensor network," in *Proc. IEEE ICIA 2010*, Harbin, China, June 2010, pp. 1532–1537.